Fusion Engineering and Design 112 (2016) 360–366

Contents lists available at ScienceDirect

Fusion Engineering and Design

journal homepage: www.elsevier.com/locate/fusengdes

Validation of large-angle scattering data via shadow-bar experiment

S. Ohnishi [a,*], S. Tamaki [b], I. Murata [b]

[a] National Maritime Research Institute, 6-38-1, Shinkawa, Mitaka, Tokyo 181-0004, Japan
[b] Osaka University, 1-14-16-1, Yamadaoka, Suita-si, Osaka 565-0871, Japan

HIGHLIGHTS

- An experiment to validate large-angle scattering cross section is conducted.
- Pieces of Nb foil are set behind a shadow bar to obtain the ^{92m}Nb production rates.
- The results calculated using ENDF/B-VI library data exhibit a 57% overestimation.
- The adjustment of cross section in large-angle region makes the C/E close to 1.

ARTICLE INFO

Article history:
Received 17 December 2015
Received in revised form 28 June 2016
Accepted 29 June 2016
Available online 7 July 2016

Keywords:
Nuclear data
ENDF/B-VI
JEFF-3.1
JENDL-4.0
Large-angle scattering
MCNP5

ABSTRACT

An experiment emphasizing the influence of large-angle scattering on nuclear data was conducted, in which a Fe shadow bar and a Fe slab target were placed before a deuterium–tritium fusion (DT) neutron source. Two Nb foils were set on both sides of the shadow bar in order to monitor the neutron source intensity and to measure the neutrons scattered from the slab target. The ^{93}Nb(n,2n)^{92m}Nb reaction rate of the foil was measured following the DT neutron irradiation and calculated using the MCNP5 Monte Carlo radiation transportation code. The ^{92m}Nb production rates calculated using data from the JEFF-3.1 and JENDL-4.0 libraries agreed with that measured in the experiment, while the result calculated using data from the ENDF/B-VI library exhibited a 57% overestimation. Because the sensitivity of the ^{92m}Nb production rate to the scattering angular distribution was large in the angular region between scattering direction cosines of −0.9 and −0.4, the scattering angular distribution was adjusted in that region. This adjustment resulted in a calculation-to-experiment ratio close to 1, but had little influence on the existing integral benchmark experiment.

1. Introduction

Many benchmark experiments have been conducted in order to validate nuclear data. In typical integral benchmark experiments, a slab, sphere, or cylindrical assembly is irradiated by neutrons or various materials; for example, Nb [1], Pb [2], V [3], C, or Be [4] have been subjected to such irradiation, and the results have been recorded in various large benchmark databases [5]. In particular, the data related to Fe are important for industrial purposes, and many benchmark experiments have been conducted with regard to this material [6–10].

Recent Fe benchmark experiments in the high-energy regime [11] have indicated that the differences between measured and calculated spectra become more distinct with increased detector distance from the neutron beam axis. This finding implies that the large-angle scattering cross section is questionable. Similar disagreement has also been reported for a deuterium–tritium fusion (DT) neutron beam experiment [12]. Fig. 1 shows the angular scattering cross section of ^{56}Fe for 15-MeV incident neutrons in ENDF/B-VI [13], JEFF-3.1 [14], and JENDL-4.0 [15] libraries. It is apparent that there is little difference between the nuclear data in the forward direction, but the differences become significant in the large-angle region (>90°).

Therefore, an experiment using a Fe shadow bar and a slab Fe target irradiated by a DT neutron source is conducted in this study in order to validate the large-angle scattering cross section. The shadow bar is used in order to prevent direct contribution from the DT source. In addition, a Nb foil is set behind the shadow bar, i.e., between the shadow bar and the slab target, so as to measure the scattered neutrons. The target size is set to be less than a few DT-neutron mean free paths so as to decrease the forward scattering inside the target. The slab target is irradiated by the DT neutrons and the ^{93}Nb(n, 2n)^{92m}Nb reaction rate is measured. Then,

* Corresponding author.
E-mail address: ohnishi@nmri.go.jp (S. Ohnishi).

http://dx.doi.org/10.1016/j.fusengdes.2016.06.062
0920-3796/

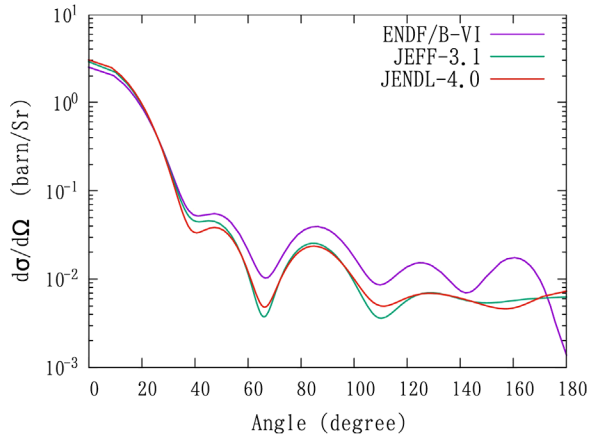

Fig. 1. Angular elastic scattering cross sections of ^{56}Fe for 15 MeV neutron according to ENDF/B-VI, JEFF-3.1, and JENDL-4.0.

the reaction rate is compared with those calculated using Monte Carlo transportation code for different data sets.

2. Methods

2.1. Geometry

In this study, the benchmark geometry consisted of a shadow bar and a slab target, both of which were composed of Fe. Nb foils were used to measure the neutrons. The shadow bar had a frustum shape so as to reduce the number of unnecessary collisions within the bar. The slab target had 10-cm thickness, which is almost identical to twice the mean free path of DT neutrons in Fe. Fig. 2 shows the geometry of the shadow-bar experiment. Two Nb foils were set on the shadow bar. One was set on the neutron source side (upper base) to facilitate monitoring of the DT source intensity, while the other was set on the slab target side (lower base) in order to measure the scattered neutrons.

2.2. Neutron source

The shadow-bar experiment was conducted at OKTAVIAN at Osaka University. A small water-cooled tritium (T) target was installed in the OKTAVIAN heavy irradiation room, and the typical neutron generation rate was approximately 1×10^{10} n/s. The water-cooled target was the same type as that used in the Japan Atomic Energy Agency (JAEA) Fusion Neutronics Source (FNS) [16]. The cup-shaped target was composed of Cu alloy, having 30-mm diameter and 20-mm height, and a Ti layer of 5 μm in thickness was deposited on the bottom of the cup. Deuterium (D) or T gas could be absorbed in the Ti layer. The angular distributions and energy spectra in both D [17] and T [18] targets have been calculated and measured, considering the kinematics of the particles in the target and the scattering in the structures; for example, the cooling pipes and water. The spectra and polar angle distribution of neutrons emitted from a T target are shown in Figs. 3 and 4, respectively.

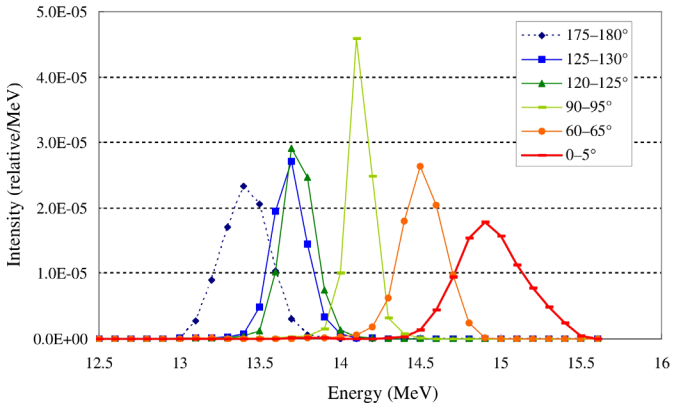

Fig. 3. DT neutron source spectra [18].

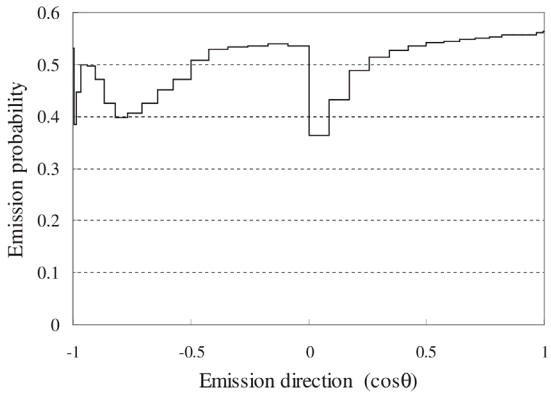

Fig. 4. DT neutron source angular distribution [18].

2.3. Neutron detector

Nb activation foils were employed for the DT neutron detection and the ^{93}Nb(n,2n)^{92m}Nb reaction rates were measured using a

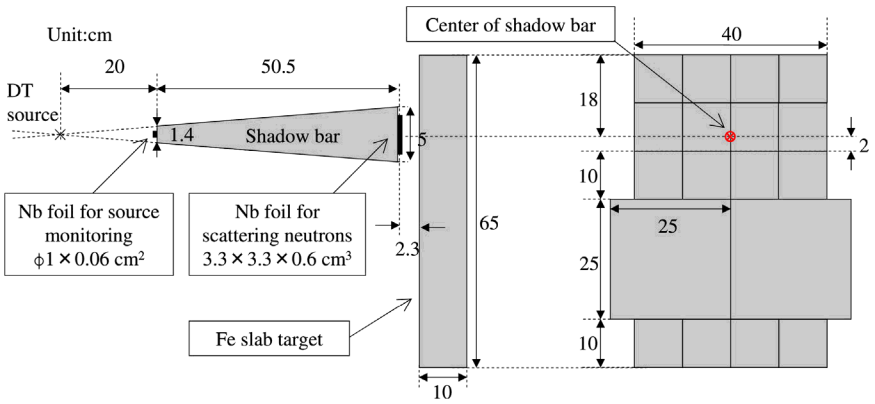

Fig. 2. Geometry of shadow-bar experiment. Side (left) and rear (right) views.

Table 1
^{93}Nb(n,2n)^{92m}Nb reactions rates per atom per source neutron. The numbers in parentheses are the numerical values of the relative error in percent. These values include the photon-counting statistical error and the systematic error of the HPGe detection efficiency (typically 5%).

Geometry	Reaction rate
With Fe slab target	3.01×10^{-31} (9.0%)
Without slab	1.59×10^{-31} (9.2%)
Difference	1.42×10^{-31} (12.1%)

high-purity Ge (HPGe) detector. In the shadow-bar experiment, two types of Nb foils were used. A small foil, a disk of 1-cm diameter and 0.06-cm thickness, was set on the upper base of the shadow bar in order to monitor the absolute neutron source strength. This foil was employed because no detector for the associated charged particle is available in OKTAVIAN. A larger foil ($3.3\times3.3\times0.6\,cm^3$) was set on the lower base of the shadow bar in order to measure the neutrons scattered from the slab Fe target.

3. Experimental results

3.1. Reaction rate

To eliminate the contribution of the neutrons scattered by the structures in the irradiation room or by the wall of the room itself, the "net" reaction rate of the large Nb foil was acquired in two steps. First, the shadow bar, slab target, and Nb foils were exposed to the DT neutrons, and the numbers of activated Nb atoms in both types of the Nb foils were counted by the HPGe detector, and the reaction rate of the large Nb foil was estimated. Second, DT neutron irradiation was conducted after the Fe slab target was removed and the Nb foils were set again. The ^{92m}Nb count was obtained in the same manner in order to estimate the contribution from the neutrons scattered by the room wall. Hence, the net ^{93}Nb(n, 2n)^{92m}Nb reaction rate of the large Nb foil was obtained by subtracting the above components. The DT irradiation was performed for 6.7 h with a slab target and 6.3 h without a slab target, and the generated neutron counts were 1.49×10^{14} and 1.39×10^{14}, respectively. The neutron source intensity was estimated based on the ^{92m}Nb production rate of the small Nb foil set on the upper side of the shadow bar using the DT-energy-averaged ^{92m}Nb production cross section of 0.464 barn (±4.2%) [19], assuming an uncollided flux from an isotropic source. The neutron source intensity is expressed as

$$n_{source} = \frac{4\pi r^2}{\sigma(1-e^{-\lambda\Delta t})} n_{small}, \quad (1)$$

where n_{source} represents the number of source neutrons per unit time, r is the distance between the neutron source and the small Nb foil, σ is the DT-energy-averaged ^{92m}Nb production cross section, λ is the ^{92m}Nb decay constant, Δt is the irradiation time, and n_{small} indicates the ^{93}Nb(n, 2n)^{92m}Nb reactions per target atom per unit time of the small Nb foil. The deuteron beam current was approximately 290 μA and was almost constant during the experiments. Table 1 summarizes the measured reaction rate of the Nb foil per atom per source neutron. The net ^{93}Nb(n,2n)^{92m}Nb reaction rate of the large Nb foil was 1.42×10^{-31} (12.1%).

3.2. Normalized reaction rate

To compare the experiment and calculation, a normalized quantity should be used that does not depend on the amount of neutrons generated in the source. Usually, the reaction rates per source neutron summarized in Table 1 are adopted for the activation foil method. In this experiment, a small Nb foil was set near the T target for source monitoring, because the associated alpha particle technique cannot be used in OKTAVIAN. However, the small Nb foil measurement includes the contribution of the neutrons backscattered from the shadow bar. Thus, the generated neutron count estimated from the radioactivity of the small Nb foil and the flux density of the uncollided isotropic source particles is overestimated. In fact, the source neutron per reaction rate of the small Nb foil was found to be 1.08×10^{28}, from Eq. (1) and under the conditions: $r = 20$ cm; $\sigma = 0.464$ barn; $\lambda = 7.90\times10^{-7}\,s^{-1}$; and $\Delta t = 23{,}400$ s. In contrast, that calculated using the Monte Carlo simulation was 1.05×10^{28}. Hence, the calculation-to-experiment ratio (C/E) was also overestimated by 3%, if the source neutron count estimated using the small Nb foil was adopted as the normalization factor.

Therefore, the reaction rate of the small foil itself was adopted as the normalization factor in this study. The radioactivity of the small Nb foil was exactly proportional to the amount of neutrons generated in the T target if decay correction was applied, and its proportional constant did not vary depending on the presence or absence of the slab target, although it did include the contribution of the neutrons backscattered from the shadow bar. However, because the backscattered neutron contribution was considered in the same manner in the Monte Carlo simulation, the C/E ratio of the normalized reaction rate was not biased by the backscattered neutrons. Further, the difference in the normalization factors given by the various nuclear data libraries is less than 0.3%, and it can be ignored. Therefore, the normalized reaction rate, which is the ratio of the large to small Nb foils, is suitable for comparison of the experimental data with those of the Monte Carlo simulation. Furthermore, this normalized reaction rate does not include the uncertainty of the ^{92m}Nb production cross section. Here, the normalized reaction rate is defined as

$$\text{Normalized reaction rate} \equiv \frac{n_{large}}{n_{small}}, \quad (2)$$

where n_{large} is the number of ^{92m}Nb atoms per target atom in the large Nb foil set on the lower base of the shadow bar, and n_{small} is that of the small Nb foil set on the upper base. The uncertainty of the source strength is canceled by eliminating an equal factor on the denominator and numerator. In addition, the systematic error of the HPGe is also canceled when the same HPGe detector is used for both foils. The reaction rates per atom are summarized in Table 2. Hence, we concluded that the net normalized reaction rate was 1.51×10^{-3} (11.3%) in this shadow-bar experiment.

3.3. Monte Carlo calculation

The reaction rates of the Nb foils were calculated using the MCNP5 [20] Monte Carlo radiation transportation calculation code and data from three different nuclear libraries: ENDF/B-VI [13], JEFF-3.1 [14], and JENDL-4.0 [15]. The shadow-bar geometry shown

Table 2
Normalized reaction rate. The numbers in parentheses are the systematic and statistical errors of the HPGe measurements.

	Small Nb foil for source monitoring	Large Nb foil for neutron scattering	Normalized reaction rate
With Fe slab	1.40×10^{-14} (5.5)	4.46×10^{-17} (5.6)	3.19×10^{-3} (7.9)
Without Fe slab	1.31×10^{-14} (5.4)	2.20×10^{-17} (6.2)	1.68×10^{-3} (8.2)
Difference			1.51×10^{-3} (11.3)

Table 3
Calculated ^{93}Nb(n,2n)^{92m}Nb reaction rates and normalized reaction rates. The numbers in parentheses are the statistical errors (unit: %).

Library	Small Nb foil for source monitoring	Large Nb foil for scattering neutrons	Normalized reaction rate
ENDF/B-VI	9.56×10^{-29} (0.03)	2.28×10^{-31} (0.37)	2.38×10^{-3} (0.37)
JEFF-3.1	9.53×10^{-29} (0.03)	1.44×10^{-31} (0.47)	1.51×10^{-3} (0.46)
JENDL-4.0	9.53×10^{-29} (0.03)	1.51×10^{-31} (0.44)	1.59×10^{-3} (0.44)

Table 4
Normalized reaction rates and C/Es.

	Normalized reaction rate	C/E
Experiment	1.51×10^{-3} (11.3)	–
ENDF/B-VI	2.38×10^{-3} (0.37)	1.57 (11.3)
JEFF-3.1	1.51×10^{-3} (0.46)	1.00 (11.3)
JENDL-4.0	1.59×10^{-3} (0.44)	1.05 (11.3)

in Fig. 2 was simulated in the transportation calculation, and the JENDL/D-99 dosimetry library [21] was used for the ^{92m}Nb production cross section. The source energy spectrum and the polar distribution of the emitted neutron were adopted from the JAEA/FNS data described in Section 2.2. In this simulation, the effect of scattering from the room wall was not considered, because this effect was eliminated from the experimental results by subtracting the data obtained without the slab target from those obtained with the slab target. The calculated reaction rates of each foil are shown in Table 3. In addition, the C/Es obtained for each nuclear data library data set are summarized in Table 4. The normalized reaction rates calculated with data from JEFF-3.1 or JENDL-4.0 agreed well with those of the experiment. However, the results obtained using the ENDF/B-VI data exhibited overestimation by a factor of 1.57. It is remarkable that such a significant discrepancy arises between modern nuclear data sets for such a simple experimental configuration.

4. Discussion

4.1. Nuclide specification

Natural Fe consists of four stable isotopes: ^{54}Fe, ^{56}Fe, ^{57}Fe, and ^{58}Fe. We first specified the nuclide that causes the overestimation of C/E in the ENDF/B-VI data. For this purpose, the Nb foil reaction rate was calculated again, with the ENDF/B-VI data for each Fe isotope being replaced with those given by JENDL-4.0. The calculated normalized reaction rates of the Nb foil and the C/Es are summarized in Table 5. The C/E became approximately 1 when the ^{56}Fe data were replaced by those from JENDL-4.0, and the data for the other nuclides had little influence on the normalized reaction rate. These results show that the difference between the nuclear data libraries is caused by the data for ^{56}Fe, and that the ^{56}Fe data in the ENDF/B-VI library are problematic.

4.2. Energy and angular region

The calculation in the previous subsection clearly indicates that the discrepancy between the different data sets and the

Table 5
Normalized reaction rates when the ENDF/B-VI data for each Fe nuclide are replaced by those from JENDL-4.0. The numbers in parentheses are the systematic and statistical errors in percent.

Exchanged nuclide	Normalized reaction rate	C/E
None (original)	2.38×10^{-3} (0.29)	1.57 (11.3)
^{54}Fe	2.35×10^{-3} (0.29)	1.56 (11.3)
^{56}Fe	1.63×10^{-3} (0.34)	1.08 (11.3)
^{57}Fe	2.38×10^{-3} (0.29)	1.58 (11.3)
^{58}Fe	2.38×10^{-3} (0.29)	1.58 (11.3)

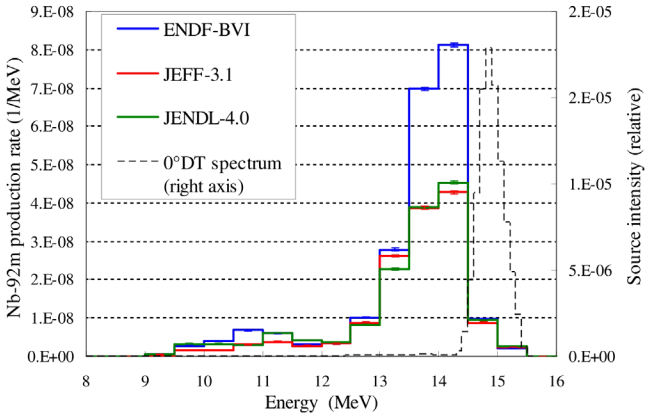

Fig. 5. ^{92m}Nb production rate of large Nb foil (left axis) and neutron spectrum emitted at 0° (right axis).

experimental data is due to the ^{56}Fe data. The energy and angular ranges for which this discrepancy occurs are identified in this subsection. For this purpose, the energy dependence of the ^{92m}Nb production rate of the large Nb foil was calculated, as shown in Fig. 5.

The ^{92m}Nb production rates have a peak between 13.5 and 14 MeV, where the differences between the nuclear data libraries become large. For backward scattering ($\cos\theta$=−1) by ^{56}Fe, the energy of the scattered neutrons becomes $(55/57)^2$ of the incident energy. In particular, 13.5 MeV corresponds to the energy of 14.7-MeV neutrons scattered through 113° ($\cos\theta$=−0.4) in a classical two-body collision. Therefore, the ^{92m}Nb production rate peak in Fig. 5 is regarded as being composed of the neutrons scattered through a large angle of more than 113° in the slab target, and the discrepancy problem is assumed to lie within the large-angle scattering cross section.

In the ACE file format [22], the scattering angular distribution is stored as the probability distribution function (PDF) and the cumulative distribution function (CDF). Figs. 6 and 7 show the elastic

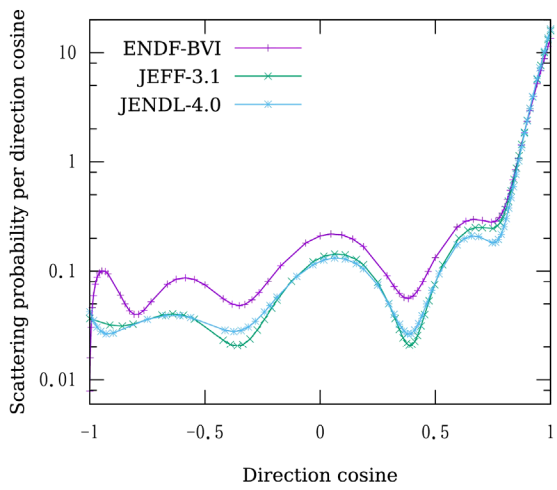

Fig. 6. Elastic scattering angular probability of ^{56}Fe for 15-MeV neutrons.

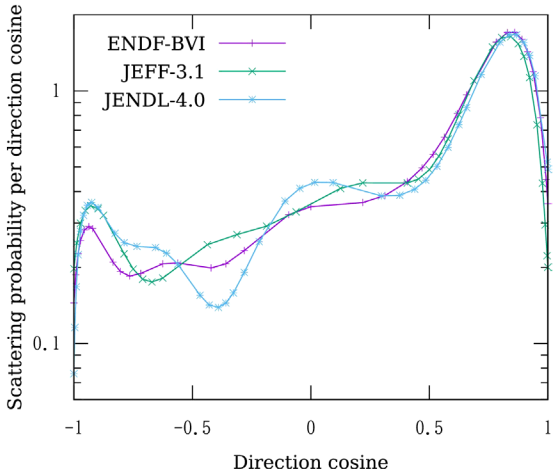

Fig. 7. Inelastic scattering angular probability of ^{56}Fe at first excited state for 15-MeV neutrons.

and inelastic scattering angular probabilities given by ENDF/B-VI, JEFF-3.1, and JENDL-4.0.

In Table 4, the normalized reaction rates and C/Es calculated using the JEFF-3.1 and JENDL-4.0 data are in agreement; however, the results obtained using the ENDF/B-VI data differ significantly. The elastic scattering angular probability also exhibits the same tendency, with the C/Es in the large-angle region obtained using the JEFF-3.1 and JENDL-4.0 data being similar, whereas the results from the ENDF/B-VI data are different. Therefore, an adjustment of the elastic scattering angular probability was attempted in this work.

4.3. Sensitivity

Prior to adjustment of the elastic scattering angular probability of ^{56}Fe, the sensitivity of the large Nb foil was estimated. The MCNP5 "PERT" card can analyze the sensitivities of tallies to the material density or each reaction cross section; however, the angular distribution is not supported by that card. Hence, the sensitivity of the scattering angular probability was estimated by modifying an MCNP5 subroutine.

The point detector in the MCNP5 code obtains the contribution from each scattering to the flux according to [22]

$$F = w\frac{p(\mu)}{2\pi R^2}\,\mathrm{e}^{-\int_0^R \Sigma_t(s)\mathrm{d}s}, \tag{3}$$

where μ is the direction cosine of the incident velocity and the position vector from the collision point to the tally, p is the scattering angular probability, F is the contribution to the tally, w is the particle weight, R is the distance from the collision point to the tally, Σ_t is the macroscopic total cross section, and s is the position along R. Then, the sensitivity to p is obtained via partial differentiation with respect to p, such that

$$\frac{\partial F}{\partial p} = \frac{w}{2\pi R^2}\,\mathrm{e}^{-\int_0^R \Sigma_t(s)\mathrm{d}s}. \tag{4}$$

MCNP5 has a subroutine called "tallyx," which is called whenever a tally event occurs, provided it is enabled by the FU card [20]. The tallyx subroutine is empty by default, and user-defined routines can be executed after implementation and recompilation. The sensitivity of the large Nb foil in the shadow-bar experiment to the scattering angular probability of ^{56}Fe was calculated using the tallyx subroutine and Eq. (4), and the results are shown in Fig. 8. The sensitivity is significant for forward ($\cos\theta = 0$) and large-angle ($\cos\theta = -0.9$ to -0.4) scattering. As described in Section 4.2,

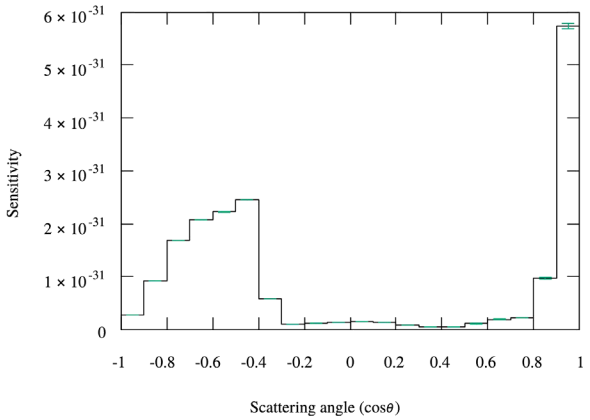

Fig. 8. ^{56}Fe sensitivity to elastic scattering angular probability.

provided that the ^{93}Nb(n,2n)^{92m}Nb reaction is caused by single scattered neutrons, the ^{92m}Nb atoms in the large Nb foil are produced by the neutrons scattered through angles larger than 113°. The result of this sensitivity analysis supports the conclusion given in Section 4.2.

4.4. Cross section adjustment

The large-angle part of the elastic scattering probability of ^{56}Fe in the ENDF/B-VI data was selected for adjustment. Two kinds of adjustment of the ENDF/B-VI ^{56}Fe data were tested, i.e., adjustment of the elastic scattering angular probability of ^{56}Fe for 15-MeV neutrons by: (1) replacing the entirety of the angular distribution with the corresponding data from JENDL-4.0 (hereafter referred to as "whole adjustment"); (2) replacing the large-angle part ($\cos\theta = -0.9$ to -0.4) only with the JENDL-4.0 data (referred to as "partial adjustment"). Both the adjusted and original elastic scattering angular probabilities are shown in Fig. 9. The normalized reaction rates were calculated in the shadow-bar experiment geometry using the wholly and partially adjusted ENDF/B-VI data, and the results are summarized in Table 6. Both adjustments yielded C/Es close to 1.

4.5. Influence of adjustments on past integral benchmark experiment

The elastic scattering angular distribution was adjusted and the C/Es in the shadow-bar experiment were altered dramatically. Note that a number of adjustment methods may yield C/E values close

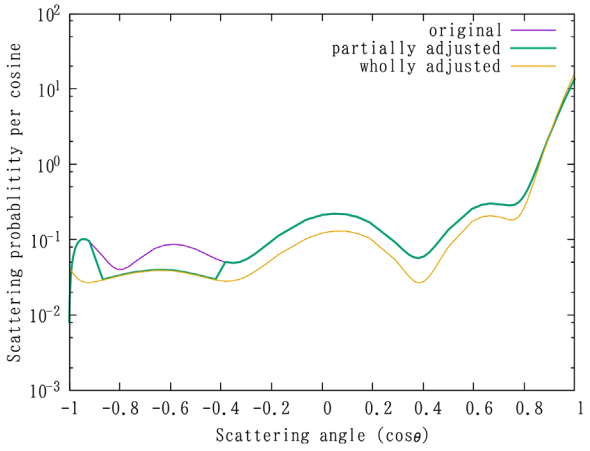

Fig. 9. Adjusted and original elastic scattering angular probabilities of ^{56}Fe for 15-MeV neutrons.

Table 6
Normalized reaction rates for adjusted nuclear data. The numbers in parentheses are the systematic and statistical errors in units of percent.

Data	Normalized reaction rate	C/E
ENDF/B-VI (original)	2.38×10^{-3} (0.37)	1.58 (11.3)
ENDF/B-VI (wholly adjusted)	1.74×10^{-3} (0.64)	1.15 (11.3)
ENDF/B-VI (partially adjusted)	1.94×10^{-3} (0.61)	1.28 (11.3)

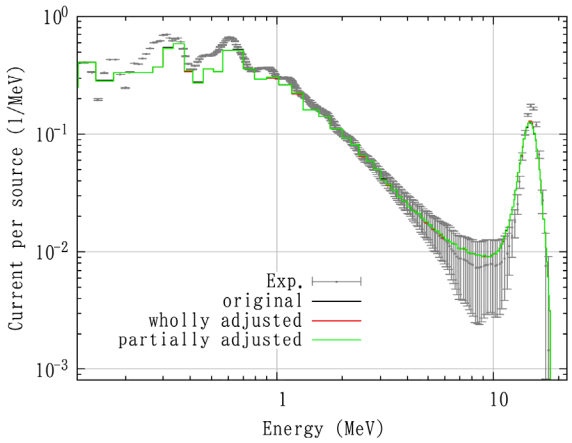

Fig. 10. Spectra calculated using MCNP5 for original, partially adjusted, and wholly adjusted ENDF/B-VI data. The dots with error bars represent the measured spectrum. All the calculated spectra closely overlap along the same line.

to unity. However, the adjusted nuclear data should reproduce the results of the previous integral benchmark experiment; therefore, the adjusted data were confirmed against the results for the Institute of Physics and Power Engineering (IPPE) Fe-shell benchmark experiment [7].

In that experiment, a DT neutron source was placed at the center of a 7.5-cm-thick Fe spherical shell having an outer radius of 12 cm, and the neutron spectrum on the outer surface was measured. Fig. 10 shows the calculated spectra obtained using MCNP5, for original, partially adjusted, and wholly adjusted ENDF/B-VI data. All the calculated spectra coincided to within 4%, and the adjustments had little influence on the reproducibility of the Fe-shell benchmark experiment.

5. Conclusion

A new experiment that focused on the large-angle scattering cross section was conducted, in which Nb foils were set on the edges of a shadow bar. The ^{93}Nb(n,2n)^{92m}Nb reaction rates of each foil were measured by a HPGe detector, and were also calculated using MCNP5 with data from the ENDF/B-VI, JEFF-3.1, and JENDL-4.0 libraries. The ^{92m}Nb production reaction rates calculated using the JEFF-3.1 and JENDL-4.0 data agreed with that measured in the experiment. However, the results obtained using the ENDF/B-VI data were 1.6 times that calculated using the JEFF-3.1 data, even though the geometry of the shadow-bar experiment was rather simple. Note that, apart from the alpha-particle production cross sections, the neutron incident data for ^{56}Fe in ENDF/B-VII [10] do not differ dramatically from those of ENDF/B-VI; therefore, this problem persists. Because the sensitivity of the ^{92m}Nb production rate to the scattering angular distribution was large in the region for which the direction cosine is between −0.9 and −0.4, the elastic scattering angular distribution obtained for the ENDF/B-VI data was adjusted in that region. When the adjusted nuclear data were employed, the C/E ratios became close to 1. In addition, it was confirmed that the adjustment had little influence on the existing integral benchmark experiment. In other words, the shadow-bar experiment validated the large-angle scattering cross section data. Note that this check was not performed in the conventional integral benchmark experiment. Through the shadow-bar experiment conducted in this work, it has been revealed that the nuclear data for such an ordinary material as Fe are problematic. Thus, the data for the advanced materials employed in fusion reactors may also be problematic within the large-angle scattering cross section regime, and further related experiments are necessary.

Acknowledgments

The authors thank Chikara Konno for insightful suggestions regarding the problems with the nuclear data. The authors are particularly grateful for the experimental support provided by the staff at OKTAVIAN, namely, Atsushi Datemichi and Hisashi Sugimoto. Without the help of the students in the Murata Laboratory at Osaka University, namely, Masanobu Manabe, Yuki Ohtani, Keita Uehara, and Naoya Hayashi, this work would not have been possible.

References

[1] C. Ichihara, S.A. Hayashi, I. Kimura, J. Yamamoto, A. Takahashi, Measurement of leakage neutron spectra from a spherical pile of niobium bombarded with 14 MeV neutrons and validation of its nuclear data, J. Nucl. Sci. Technol. 38 (11) (2001) 959–966, http://dx.doi.org/10.1080/18811248.2001.9715123.
[2] O. Kentaro, K. Keitaro, O. Seiki, T. Kosuke, S. Satoshi, A. Yuichi, K. Chikara, S. Chihiro, Y. Takahiro, DT neutronics benchmark experiment on lead at JAEA-FNS, J. Korean Phys. Soc. 59 (23) (2011) 1953, http://dx.doi.org/10.3938/jkps.59.1953 http://www.kps.or.kr/jkps/abstract_view.asp?articleuid=C94FA38C-D33B-47B5-92B3-6FE2171FE05D.
[3] F. Maekawa, Y. Kasugai, C. Konno, I. Murata, M. Kokooo, Y. Wada, Y. Oyama, A. Ikeda, Takahashi, Benchmark experiment on vanadium with D–T neutrons and validation of evaluated nuclear data libraries by analysis of the experiment, J. Nucl. Sci. Technol. 36 (3) (1999) 242–249, http://dx.doi.org/10.1080/18811248.1999.9726204.
[4] Y. Oyama, S. Yamaguchi, H. Maekawa, Experimental Result of Angular Neutron Flux Spectra Leaking from Slabs of Fusion Reactor Candidate Materials(I), JAERI-M 90-092, Japan Atomic Energy Research Institute, Tokai, Ibaraki, 1990.
[5] I. Kodeli, E. Sartori, B. Kirk, SINBAD shielding benchmark experiments status and planned activities, in: Proceedings of 14th Biennial Topical Meeting of the Radiation Protection and Shielding Division, Carlsbad, New Mexico, 2006 https://www.oecd-nea.org/science/wprs/shielding/sinbad/RPSD2006-sinbad.pdf.
[6] K. Sumita, A. Takahashi, H. Hashikura, Y. Oka, S. An, Measurements of Neutron Leakage Spectra from 50.32 cm Radius Iron Sphere, OKTAVIAN Report A-83-07, Osaka University, Suida, Osaka, 1983.
[7] S.P. Shimakov, A.A. Androsenko, P.A. Androsenko, B.V. Devkin, M.G. Kobozev, A.A. Lychagin, V.V. Sinitca, V.A. Talalaev, D.Y. Chuvilin, A.A. Borisov, V.A. Zagryadsky, 14 MeV facility and research in IPPE Talk presented at International Workshop on Fusion Neutronics Experiments, in: Proceedings of International Workshop, Fusion Neutronics Experiments INDC(CCP)-351, IAEA, Frascati, Italy, 1993 https://www-nds.iaea.org/publications/indc/indc-ccp-0351/.
[8] S.H. Jiang, H. Werle, Measurement and calculation of californium-252 fission neutron-induced gamma fields in iron, Nucl. Sci. Eng. 66 (3) (1978) 354–362 http://www.ans.org/store/article-27218/.
[9] M.B. Stanka, J.M. Adams, C.M. Eisenhauer, Proton recoil measurements of the ^{252}Cf fission neutron leakage spectrum from an iron sphere, Nucl. Sci. Eng. 134 (1) (2000) http://www.ans.org/pubs/journals/nse/a_2100.
[10] O. Allaoui, T.E. Bardouni, E.M. Chakir, H. Boukhal, M. Kaddour, B.E. Bakkari, S.E. Ouahdani, ENDF/B-VII.0, JEFF-3.1 and JENDL-4 iron and water cross sections analysis using the PCA-REPLICA shielding, Univ. J. Phys. Appl. 8 (2) (2014) 96–102, http://dx.doi.org/10.13189/ujpa.2014.020207 http://www.hrpub.org/journals/article_info.php?aid=1268.
[11] H. Nakashima, N. Nakao, S. Tanaka, T. Nakamura, K. Shin, S. Tanaka, S. Meigo, Y. Nakane, H. Takada, Y. Sakamoto, M. Baba, Experiments on Iron Shield Transmission of Quasi-Monoenergetic Neutrons Generated by 43 and 68 MeV Protons via the ^{7}Li(p,n) Reaction, JAERI-Data/Code 96-005, JAERI, Tokai, Ibaraki, 1996 http://jolissrch-inter.tokai-sc.jaea.go.jp/pdfdata/JAERI-Data-Code-96-005.pdf.
[12] S. Ohnishi, K. Kondo, T. Azuma, S. Sato, K. Ochiai, K. Takakura, I. Murata, C. Konno, New integral experiments for large angle scattering cross section data benchmarking with DT neutron beam at JAEA/FNS, Nucl. Eng. Des. 87 (5–6) (2012) 695–699, http://dx.doi.org/10.1016/j.fusengdes.2012.02.002 http://linkinghub.elsevier.com/retrieve/pii/S0920379612000579.
[13] R.F. Rose, Compiler and Editor, ENDF-201: ENDF/B-VI Summary Documentation, Tech. Rep. BNL-NCS-17541, Brookhaven National Laboratory, 1991.
[14] A.J. Koning, M. Avrigeanu, V. Avrigeanu, P. Batistoni, E. Bauge, M.-M. B, P. Bem, D. Bernard, O. Bersillon, A. Bidaud, O. Bouland, A. Courcelle, C.J. Dean, P.

Dos-Santos-Uzarralde, B. Duchemin, I. Duhamel, M.C. Duijvestijn, E. Dupont, U. Fischer, R.A. Forrest, F. Gunsing, W. Haeck, H. Henriksson, A. Hogenbirk, T.D. Huynh, R. Jacqmin, C. Jouanne, J. Keinert, M.A. Kellett, I. Kodeli, J. Kopecky, H. Leeb, D. Leichtle, J. Leppanen, O. Litaize, M.J. Lopez Jimenez, M. Mattes, E. Menapace, R.W. Mills, B. Morillon, C. Mounier, A.L. Nichols, G. Noguere, C. Nordborg, A. Nouri, R.L. Perel, P. Pereslavtsev, R.J. Perry, M. Pescarini, M. Pillon, A.J. Plompen, D. Ridikas, P. Romain, Y. Rugama, P. Rullhusen, C. de Saint Jean, A. Santamarina, E. Sartori, K. Seidel, O. Serot, S. Simakov, J.-C. Sublet, S. Tagesen, A. Trkov, S.C. van der Marck, H. Vonach, The JEFF evaluated nuclear data project, in: Proc. ND2007, EDP Sciences, 2007, p. 6, http://dx.doi.org/10.1051/ndata:07476.

[15] K. Shibata, O. Iwamoto, T. Nakagawa, N. Iwamoto, A. Ichihara, S. Kunieda, S. Chiba, K. Furutaka, N. Otuka, T. Ohasawa, T. Murata, H. Matsunobu, A. Zukeran, S. Kamada, J. Katakura, JENDL-4.0 a new library for nuclear science and engineering, J. Nucl. Sci. Technol. 48 (1) (2011) 1–30, http://dx.doi.org/10.1080/18811248.2011.9711675.

[16] C. Kutsukake, S. Tanaka, M. Kawabe, T. Suzuki, M. Yamada, T. Yamanishi, C. Konno, Prototype manufacturing of small tritium target inside JAEA, in: Proc. APFA2009 and APPTC2009, vol. 9, JSPF, Aomori, 2010, pp. 338–341.

[17] K. Kondo, K. Ochiai, C. Kutsukake, C. Konno, Characterization of the DD-Neutron Source for the 80 Degrees Beam Line of the Fusion Neutronics Source (FNS), Tech. Rep. JAEA-Technology 2008-088, JAEA, Ibaraki, 2009, http://dx.doi.org/10.11484/jaea-technology-2008-088.

[18] K. Kondo, Private communication, 2009.

[19] Y. Ikeda, C. Konno, K. Ohishi, T. Nakamura, H. Miyade, K. Kawade, H. Yamamoto, T. Kato, Activation Cross Section Measurements on Fusion Reactor Structural Materials at Neutron Energy from 13.3 to 15.0 MeV using FNS Facility, JAERI 1312, JERI, Tokai, Ibaraki, 1998.

[20] X-5 Monte Carlo Team, MCNP – A General Monte Carlo N-Particle Transport Code Version 5 Volume II User's Guide, Tech. Rep. LA-CP-03-0245, Los Alamos National Laboratory, Los Alamos, 2003.

[21] K. Kobayashi, T. Iguchi, S. Iwasaki, T. Aoyama, S. Shimakawa, Y. Ikeda, N. Odano, K. Sakurai, K. Shibata, T. Nakagawa, M. Nakazawa, JENDL Dosimetry File 99, JAERI 1344, JAERI, Tokai, Ibaraki, 2002.

[22] X-5 Monte Carlo Team, MCNP – A General Monte Carlo N-Particle Transport Code Version 5 Volume I Overview and Theory, Tech. Rep. LA-UR-03-1987, Los Alamos National Laboratory, Los Alamos, 2003.